OPEN ACCESS
Journal of Multidisciplinary Applied Natural Science Vol. 5 No. 3 (2025) https://doi.org/10.47352/jmans.2774-3047.301
Check for updates
Research Article

Effect of Solar Radiation Pressure on a Geostationary Satellite: Comparison with Spherical and Flat Models

Nindhita Pratiwi*, Dhani Herdiwijaya, Nizam Ahmad, Taufiq Hidayat, and Muhammad Isnaenda Ikhsan

Received : March 17, 2025	Revised : June 28, 2025	Accepted : July 10, 2025	Online : September 05, 2025

Abstract
Solar radiation pressure (SRP) can influence the orbital parameters of a satellite, affecting its trajectory and orbital stability. In this study, we analyze the effects of SRP on a real geostationary communication satellite using both spherical and flat models. We use three different articulation schemes: fixed solar panels (model 0), solar panels rotating about a single axis to track the Sun (model 1), and solar panels rotating about two axes for perfect Sun tracking (model 2). Among the three articulation models, model 2 showed the best overall performance with the smallest variations in SRP area (3.56%), SRP-induced force (6.44%), and torque (16.15%) due to better Sun alignment. Model 0 (fixed panels) exhibited the largest variations in SRP area (14.53%) and SRP-induced force (9.69%) but maintained stable orbital energy (0.0029%) and acceleration (0.02%). Model 1 (single-axis tracking) offered moderate improvement but had the highest torque variation (56.87%), which may affect long-term stability. Our modeling indicates that the orbital parameters of the spherical and flat models are generally similar, with a Pearson correlation coefficient of 0.9 or better. Additionally, we calculated the differences between the two models for each orbital parameter over the 10 years. The maximum differences observed are 0.022 km for the semi-major axis, 0.000017° for inclination, 0.000045 for eccentricity, 358.34° for the argument of perigee, 0.000018° for the right ascension of the ascending node, and 357.66° for the mean anomaly. We also assessed the agreement between the models and real data, showing that almost all orbital parameters for both models exhibit similar patterns to those of the real data.

Keywords: solar radiation pressure, flat model, spherical model, geostationary satellite

1. INTRODUCTION

Solar radiation pressure (SRP) originates from the interaction between the solar radiation flux and a satellite's surface through the specular and diffuse reflection of solar photons. There are two types of SRP influence: direct and indirect SRP. The acceleration due to SRP can have a variety of values, depending on the shape of the satellite, the materials on the satellite's surface, and its orientation relative to the Sun [1]-[4]. Two simple types of models have been used to determine the effects of SRP on a satellite: the spherical and the flat models. A spherical model is usually used to estimate SRP effects for objects with simple, symmetric shapes, but it becomes inaccurate for irregular or articulated structures. For more complex geometries, flat-plate models are preferred, as they approximate the satellite's surface as a combination of discrete panels, each with specific optical properties. This method enables orientation-dependent modeling of SRP-induced acceleration [5]-[7]. For example, Burnett and Schaub [5] analyzed attitude-dependent SRP forces for formation flying and control applications, showing the importance of surface articulation. Henry [6] discussed the implications of SRP for micro-thruster diagnostics in fault detection on the MICROSCOPE satellite, highlighting the operational relevance of SRP forces. Jean et al. [7] studied the impact of SRP modeling near binary asteroids, where small perturbations significantly affect orbital dynamics. These works demonstrate that SRP modeling complexity depends heavily on mission type and spacecraft configuration.

SRP can influence the orbital parameters of a satellite, affecting both trajectory and long-term stability. In addition, varying atmospheric conditions—especially during geomagnetic storms—can affect atmospheric drag and further disturb orbital parameters. Therefore, analyzing the effects of SRP is critical for both operational and long-term mission planning. In this study, we analyze the effects of SRP on a geostationary communications satellite [8]-[13]. Because SRP can perturb satellite orbits, these effects must be carefully considered in mission design and

Table 1. Satellite and simulation parameters.

Parameter	Value
Gravitational sources	Sun, Earth, Moon
Atmospheric model	Analytic
Perturbations	Drag, SRP
SRP model	Spherical, Flat
Integrator	Runge Kutta 8(9)
Time step	5 min
Relative error tolerance	10^{-9}
Semi-major axis	42166.047686373 km
Eccentricity	0.0002396315948
Inclination	0.023632580502°
Right ascension of ascending node	156.2207355081°
Argument of perigee	166.8139149308°
Mean anomaly	327.9003876072°
Satellite mass	2447 kg
Drag area	59.3952 m^2
SRP area	59.3952 m^2
Reflectivity coefficient	1.40
Specular reflectivity coefficient	0.80
Diffuse reflectivity coefficient	0.08
Coefficient of drag	2.20
Moments of inertia	$\begin{bmatrix} 764.196 & 0 & 0 \\ 0 & 50.92 & 0 \\ 0 & 0 & 740.339 \end{bmatrix}$

operations. Engineers and scientists must account for both gravitational forces from celestial bodies and non-gravitational forces such as SRP. Accurate modeling of these forces enables more reliable prediction and correction of deviations in satellite motion [14].

2. DATA AND METHODS

We obtained the input orbital parameters for the satellite we studied from CelesTrak in the format of two-line element data. To compute the SRP acting on the satellite requires solar flux data along with the geocentric satellite vector in relation to the Sun. This dataset covers the period from June 2019 to January 2023. In contrast, we compared the results from a spherical model and three different flat models over the ten-year period from June 2019 to June 2029, a timeframe chosen to align with the typical operational lifespan of geostationary satellites and to encompass the timescales over which cumulative perturbations such as SRP and orbital drift become significant. We processed these data using Python and FreeFlyer, a commercial off-the-shelf software application for space-mission design, analysis, and operations. FreeFlyer was selected for this study due to its robust capabilities and flexibility in simulating a wide range of space missions, including satellite constellations and interplanetary trajectories. Compared to other available tools, FreeFlyer offers a balance between high-fidelity modeling and an accessible scripting environment, which is particularly advantageous for customizing complex mission scenarios. Its built-in functionalities for orbit determination, maneuver planning, and coverage analysis—including SRP modeling—enable precise and efficient simulations that are essential for capturing the dynamic

behavior of satellites in various orbital environments. This comprehensive toolset significantly contributes to the accuracy and reproducibility of the results presented in this study. By default, SRP modeling is disabled in FreeFlyer, but it can be enabled easily to account for the effects of SRP on spacecraft orbits. FreeFlyer provides two SRP modeling options: spherical and flat plate. The spherical model for SRP is simpler and requires minimal setup. The flat plate model in FreeFlyer is more detailed, allowing users to configure the geometry and reflectivity of individual plates to represent the spacecraft geometry [15][16].

The spherical model estimates the effect of SRP by assuming that the satellite is a perfectly spherical object, with the same reflectivity and absorptivity coefficients everywhere on its surface. There is consequently no variation in orientation of the surface to sunlight [17]. For the spherical model, the acceleration due to SRP is given by Equation (1):

$$\boldsymbol{a}_{SRP} = \frac{S * AU^2 * C_R * A_{SRP}}{m * R^2 * c} v\,\hat{\boldsymbol{s}} \quad (1)$$

The acceleration due to SRP in the spherical model depends on several physical parameters that describe the interaction between the satellite and solar radiation. One of the key parameters is the reflectivity coefficient (C_R), a dimensionless number that quantifies the extent to which the satellite's surface reflects or absorbs sunlight. The value of C_R typically ranges between 0.0 and 2.0, where $C_R = 1$ corresponds to a "black body" that completely absorbs radiation, $C_R = 0$ represents a translucent body through which light passes unhindered, and $C_R = 2$ corresponds to a "pure mirror" that perfectly reflects radiation. Intermediate values indicate varying degrees of partial absorption and reflection. In this study, a value of $C_R = 1.4$ is used, indicating that the satellite reflects a significant portion of the incident solar flux. The higher the reflectivity coefficient, the greater the force exerted on the satellite by solar photons, and thus the more pronounced the orbital perturbation due to SRP.

The astronomical unit (AU) represents the average distance between the Earth and the Sun, approximately 1.496 x 10^{11} meters. It is used as a reference in SRP calculations to normalize the solar flux. The actual distance from the satellite to the Sun (R) varies slightly due to Earth's elliptical orbit

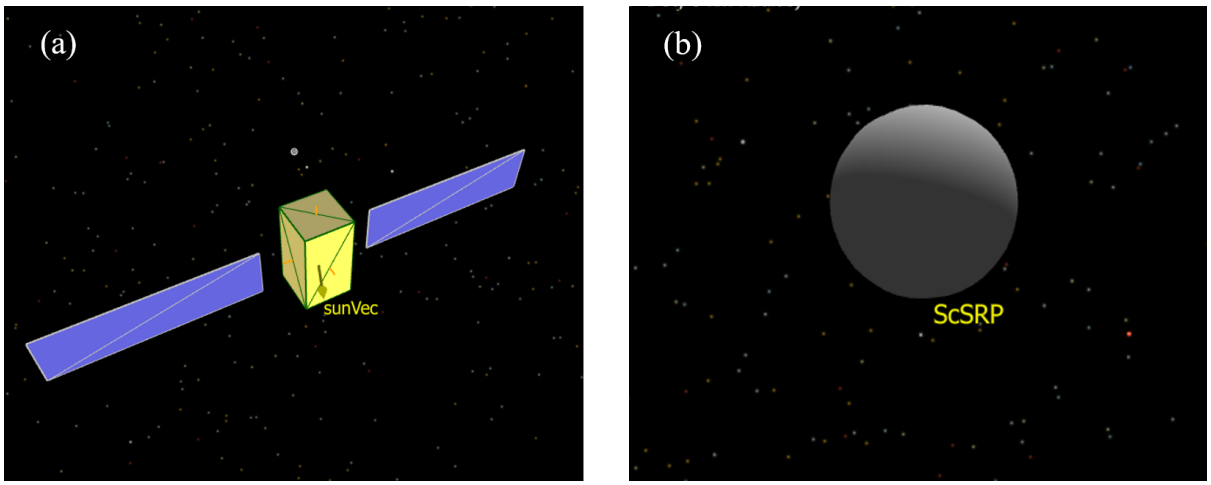

Figure 1. Satellite configurations for (a) flat and (b) spherical models in Freeflyer.

Table 2. Dimensions of the satellite model.

Parts	Dimensions
Box height	2.40 m
Box width	2.40 m
Box length	4.30 m
Wing width	2.40 m
Wing length	9.57 m

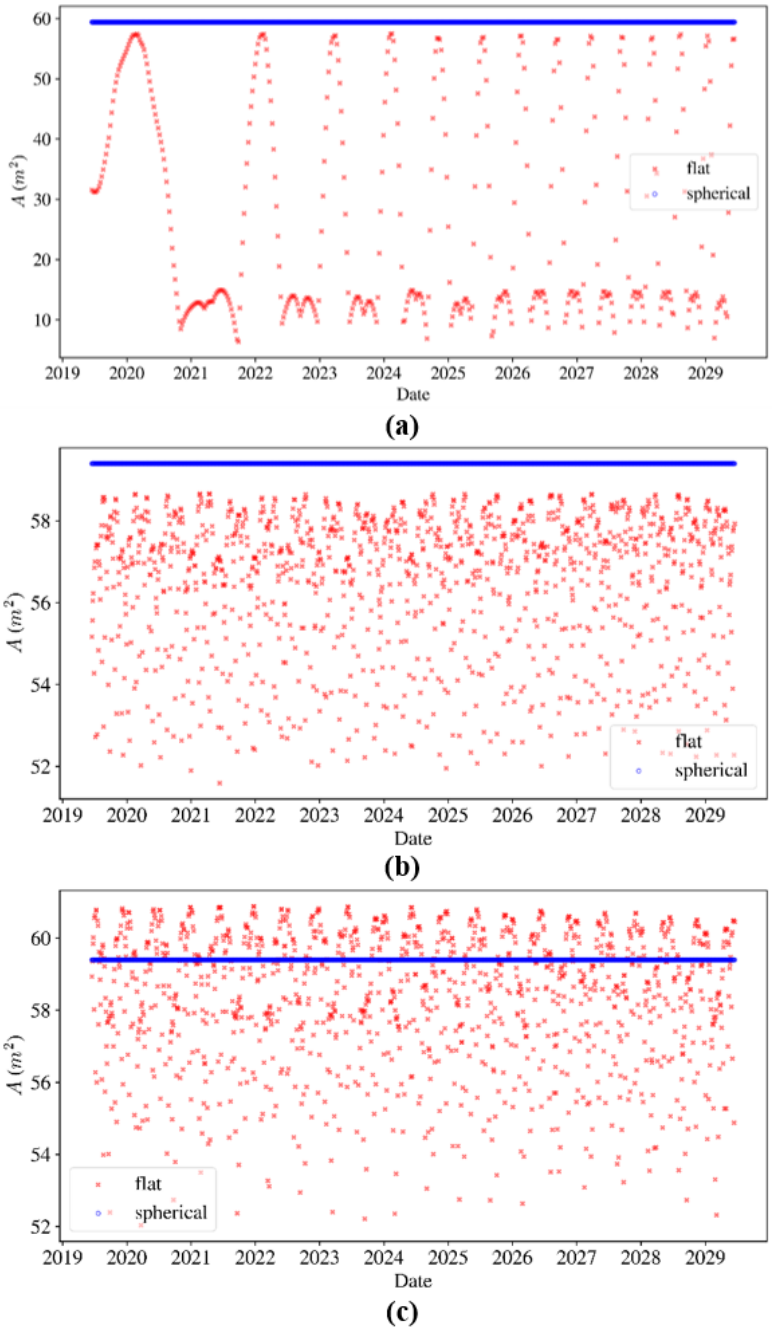

Figure 2. Comparison of SRP-effective area A over time for articulation models: (a) Model 0, (b) Model 1, and (c) Model 2 using the flat model (red) and spherical model (blue). The flat model shows dynamic variation due to satellite orientation changes, while the spherical model assumes a constant area.

and must be accounted for to accurately scale the solar flux reaching the satellite. The ratio $(AU/R)^2$ adjusts the solar pressure to the satellite's current location in the heliocentric frame. The satellite mass (m), expressed in kilograms, inversely affects the acceleration produced by SRP. A heavier satellite will experience less acceleration for a given force, making it more stable against perturbations. In contrast, low-mass satellites or CubeSats with high area-to-mass ratios are more susceptible to SRP effects. In this simulation, the satellite has a mass of 2447 kg.

The average solar flux (S) at 1 AU is approximately 1361 W/m^2 . It represents the amount of solar energy per unit area received at Earth's distance from the Sun and serves as the source term for computing SRP. This value can vary slightly depending on solar activity, but it is generally treated as a constant in orbital simulations. The speed of light (c), about 3.0 x 10^8

m/s , appears in the denominator of the SRP equation because radiation pressure is derived from the momentum of photons, which is inversely proportional to the speed of light. Therefore, it links the energy flux of sunlight to the force imparted to the satellite. The SRP cross-sectional area (A_{SRP}) is the effective area of the satellite exposed to the Sun, perpendicular to the direction of incoming solar radiation. In this study, the value is 59.3952 m^2, and it includes the surface areas of components such as the satellite body and solar panels. This parameter directly affects the magnitude of the force from SRP, a larger exposed area leads to a stronger push on the satellite.

The unit vector (ŝ) from the satellite to the Sun defines the direction in which the SRP force is applied. Because SRP is directional, this vector ensures that the acceleration is applied consistently in the correct orientation in the orbital reference frame. The eclipse factor (ν) is a dimensionless

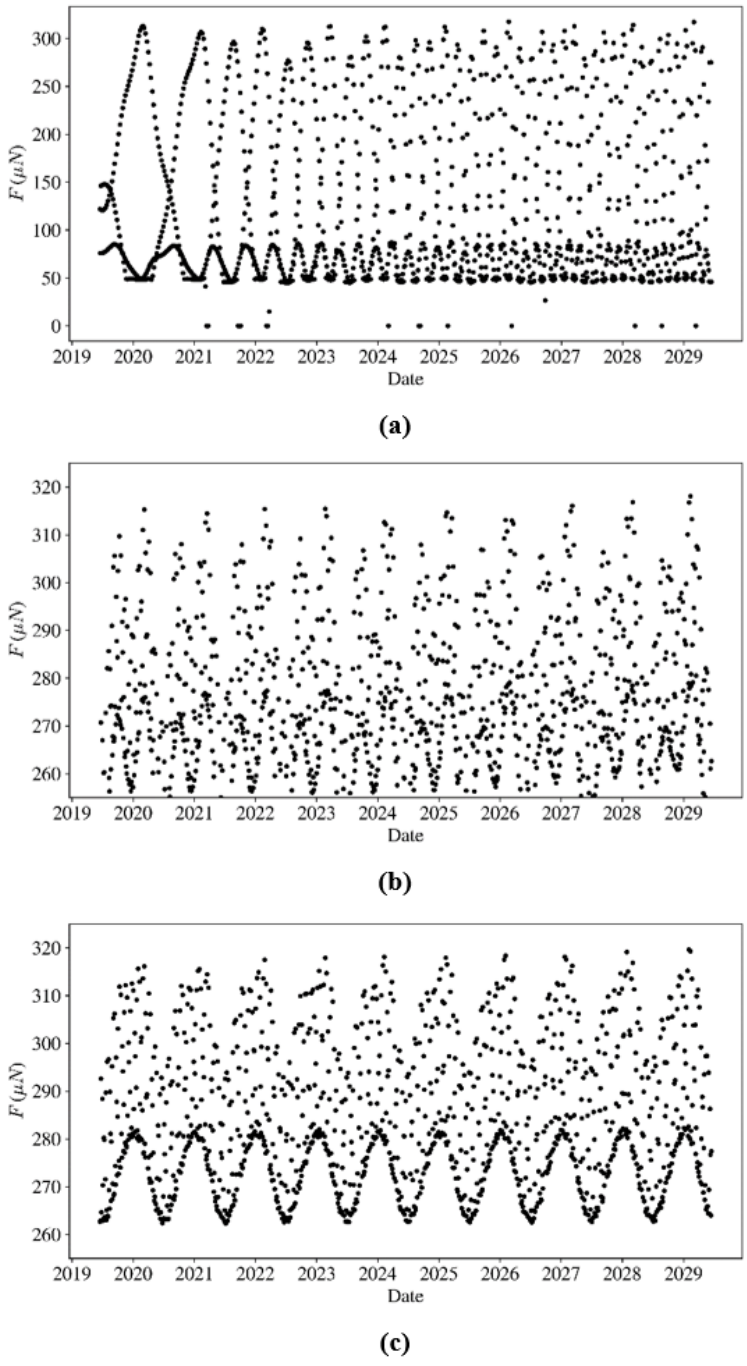

Figure 3. SRP force F (μN) acting on the satellite over time, as determined using articulation models: (a) Model 0, (b) Model 1, and (c) Model 2.

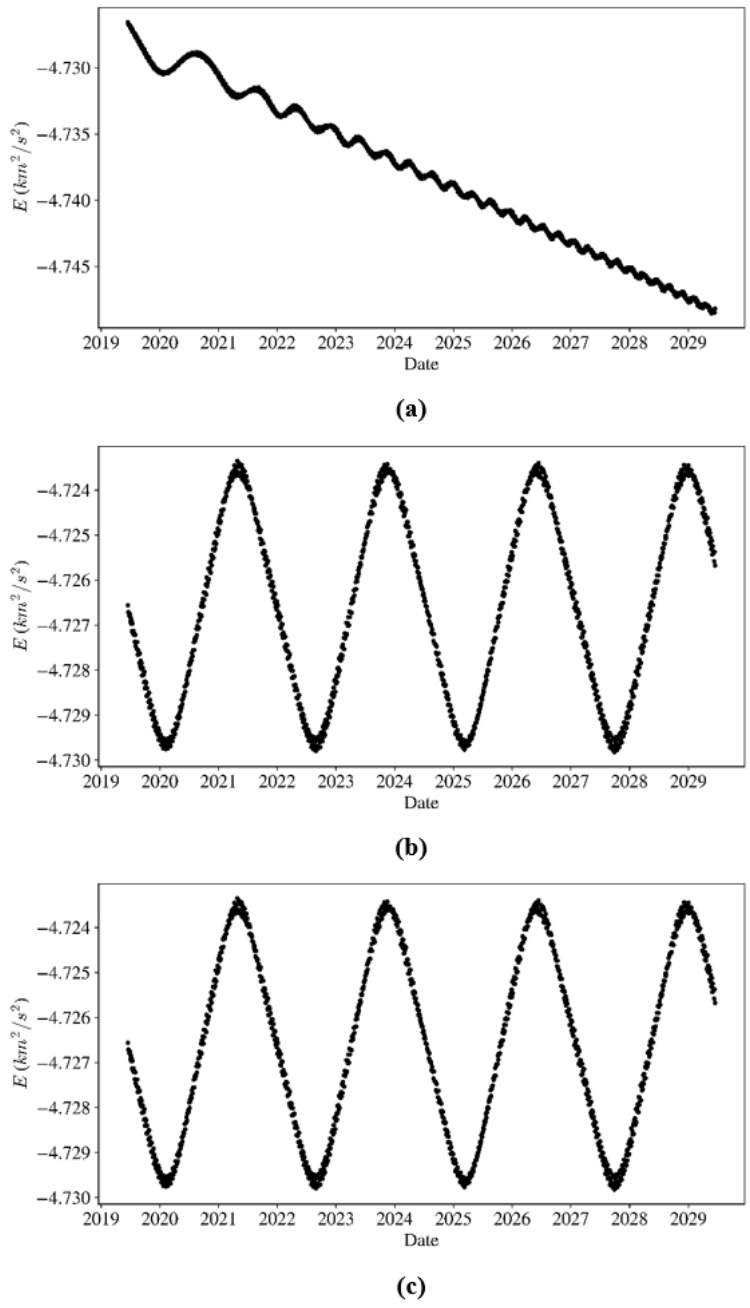

Figure 4. Orbital specific mechanical energy E over time, computed using articulation models: (a) Model 0, (b) Model 1, and (c) Model 2.

coefficient ranging from 0 to 1 , representing the amount of sunlight reaching the satellite. When the satellite is fully illuminated by the Sun, ν = 1 ; when it is in Earth's shadow (i.e., during an eclipse), ν = 0. Partial eclipse conditions yield intermediate values. This factor modulates the SRP acceleration according to the satellite's position relative to Earth and the Sun.

In contrast, the flat model discretizes the satellite's geometry into multiple planar facets, each corresponding to a specific surface of the spacecraft and characterized by individual optical properties such as specular and diffuse reflectivity. Consequently, the acceleration due to SRP varies, depending on the satellite's orientation relative to the Sun [18][19]. Equation (2) is utilized to compute the force due to the SRP acting on each plate [20]:

$$\boldsymbol{F_{SRP}} = -P_{SR} \cdot A_{plate} \cdot \left\{ 2\left(\frac{C_{r_{diffuse}}}{3} + C_{r_{specular}} \cos(\theta) \right) \hat{\boldsymbol{n}} + \left(1 - C_{r_{specular}}\right) \hat{\boldsymbol{s}} \right\} max\,(cos(\theta),0) \cdot s_{cb} \quad \textbf{(2)}$$

In the flat plate model of SRP, the force acting on a satellite is calculated by considering how individual flat surfaces respond to incoming solar photons. Each parameter in the SRP equation contributes to modeling this interaction with higher geometric and physical fidelity than the spherical model. The solar radiation pressure (P_{SR}) is the pressure exerted by sunlight at a given distance from the Sun. At 1 AU, this pressure is approximately 4.56 x 10^{-6} N/m^2 . This value can be scaled depending on the satellite's distance from the Sun using the inverse-square law. The plate area (A_{plate}) refers to the surface area of each individual panel or face of the satellite that is exposed to solar radiation. This is a critical factor in the SRP calculation because the force experienced by a

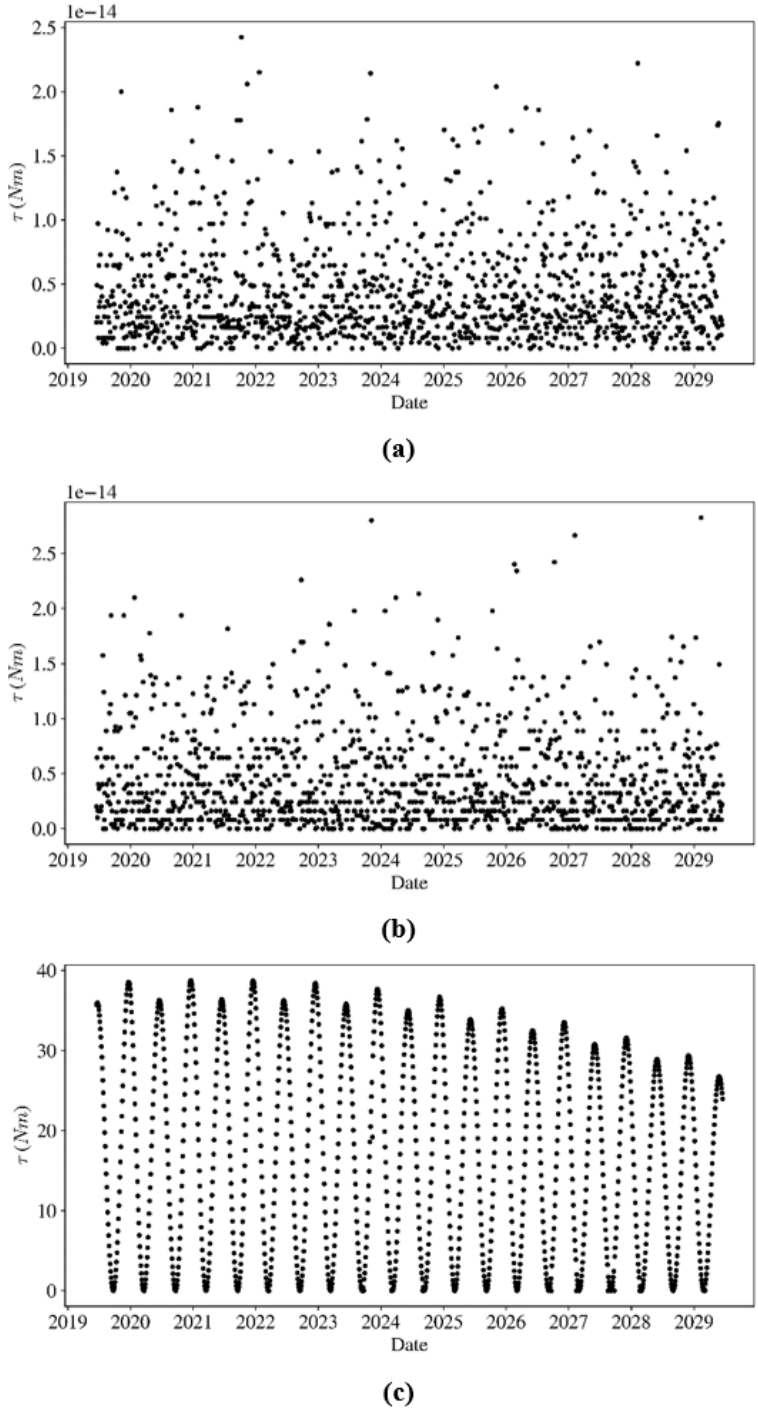

Figure 5. Torque τ (Nm) due to SRP computed using articulation models: (a) Model 0, (b) Model 1, and (c) Model 2.

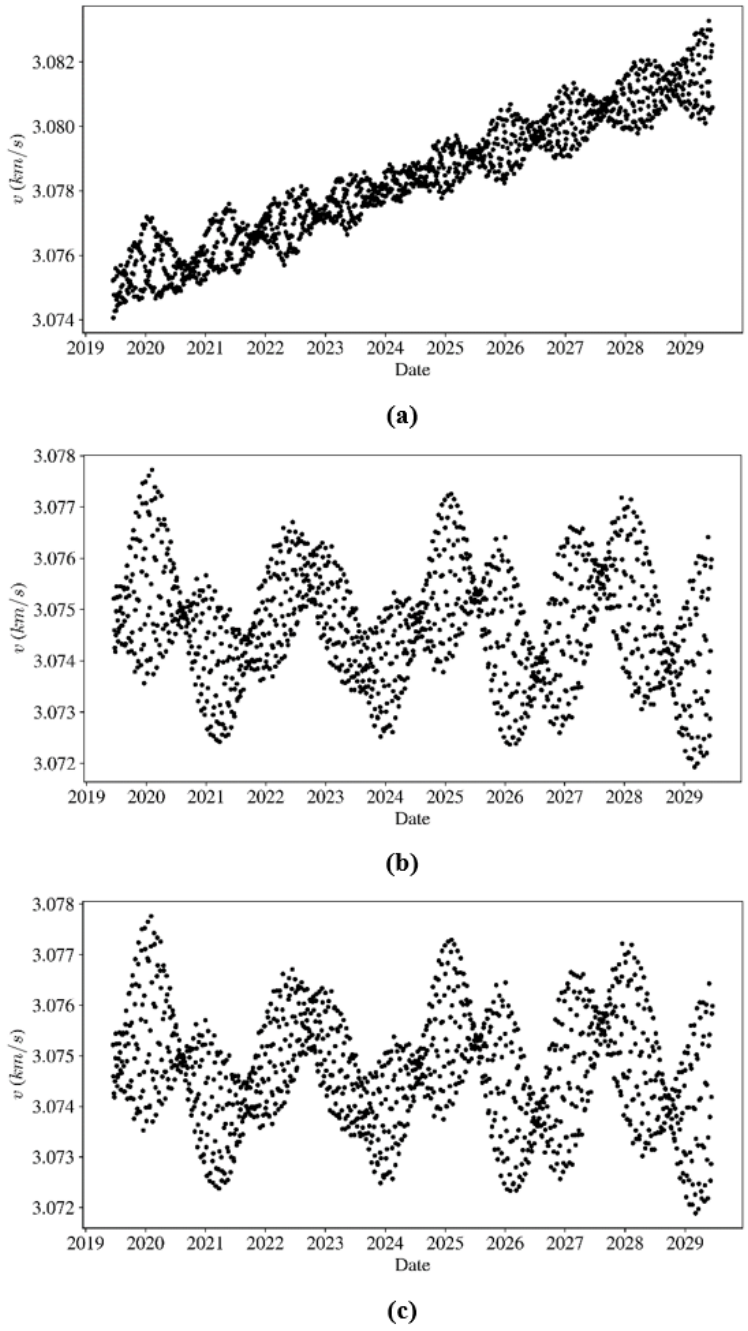

Figure 6. The variation of satellite orbital velocity ν (*km/s*) calculated on articulation models: (a) Model 0, (b) Model 1, and (c) Model 2.

surface is directly proportional to its area. Larger surfaces collect more photon momentum and therefore experience a greater SRP force. The flat model treats the satellite as a collection of such plates, each contributing separately to the net SRP force and torque.

The diffuse reflectivity coefficient ($Cr_{diffuse}$) and specular reflectivity coefficient ($Cr_{specular}$) describe how the satellite surface reflects sunlight. Specular reflection is mirror-like the incident photons reflect off the surface at the same angle as they arrived. Diffuse reflection, on the other hand, scatters the incident light in multiple directions. The sum of absorptivity, specular reflectivity, and diffuse reflectivity should not exceed 1. For instance, if a surface reflects 80% of incoming light specularly ($Cr_{specular}$ = 0.8), and 8% diffusely ($Cr_{diffuse}$= 0.08), then only 12% is absorbed. These coefficients directly affect how much momentum is transferred to the satellite from sunlight, higher reflectivity results in greater SRP-induced acceleration. The *cos* θ represents the cosine of the angle between the

incoming sunlight vector and the surface normal of the flat plate. It indicates how directly sunlight strikes the surface. A value of $cos\ \theta = 1$ means that the sunlight is perpendicular to the surface (maximum effect), while $cos\ \theta = 0$ implies that the surface is parallel to the Sun's rays and thus receives no direct radiation. This term ensures that the model accounts for the geometry of light incidence on each panel.

The unit vector N is the surface normal vector, a directional vector perpendicular to the plane of the satellite's panel. It is crucial for calculating the direction and magnitude of the force exerted by SRP on the plate, particularly when determining the projection of sunlight onto the surface. The unit vector U represents the direction from the satellite toward the Sun. Together, N and U define the orientation relationship between the plate and the Sun. The shadow coefficient (s_{cb}) accounts for whether the satellite or individual plates are in sunlight or in eclipse. It has a value between 0 and 1, when the satellite is in full sunlight ($s_{cb} = 1$) and when completely in Earth's shadow ($s_{cb} = 0$). Partial values represent partial shadowing

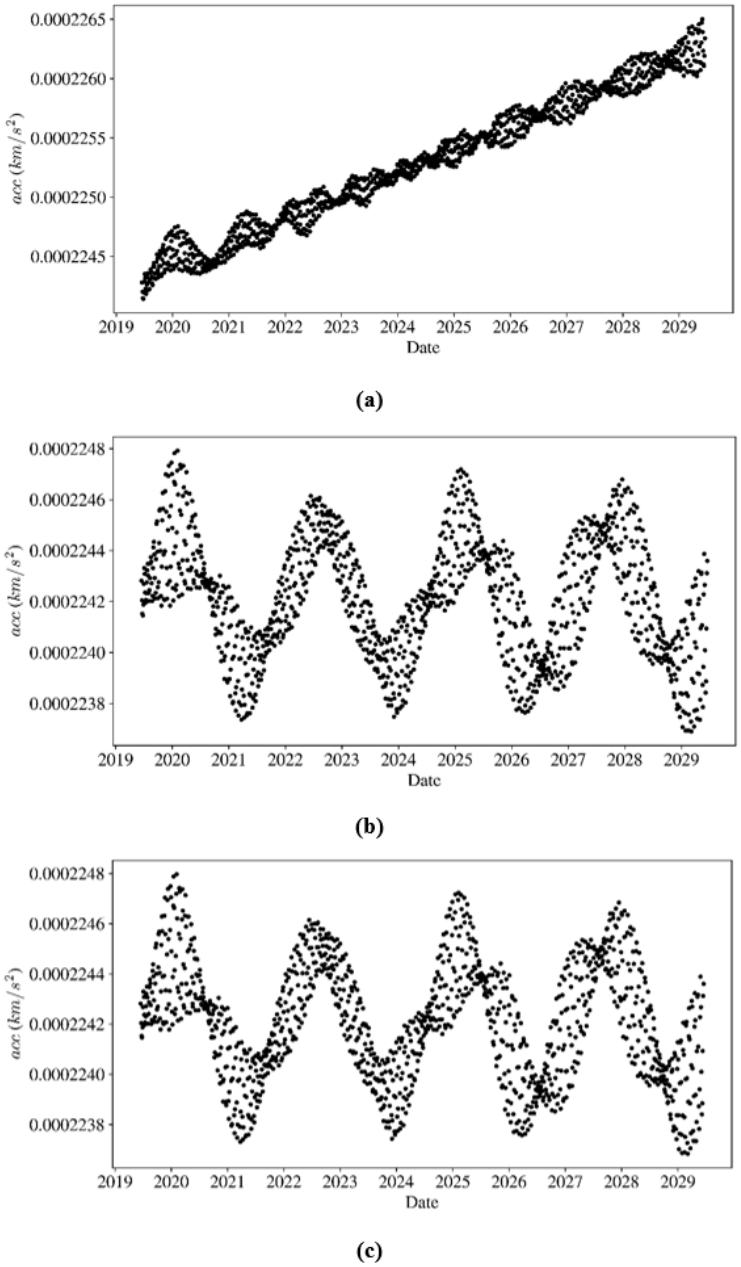

Figure 7. Acceleration due to SRP computed using articulation models: (a) Model 0, (b) Model 1, and (c) Model 2.

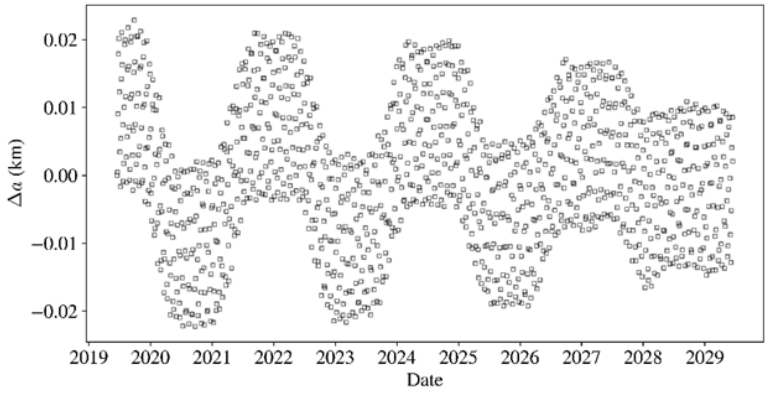

Figure 8. Difference Δa between the semi-major axes of the spherical and flat models.

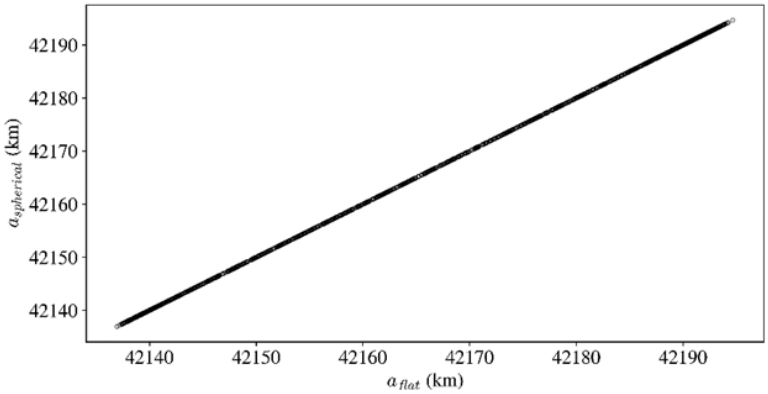

Figure 9. The relation between the semi-major axes of the spherical and flat models.

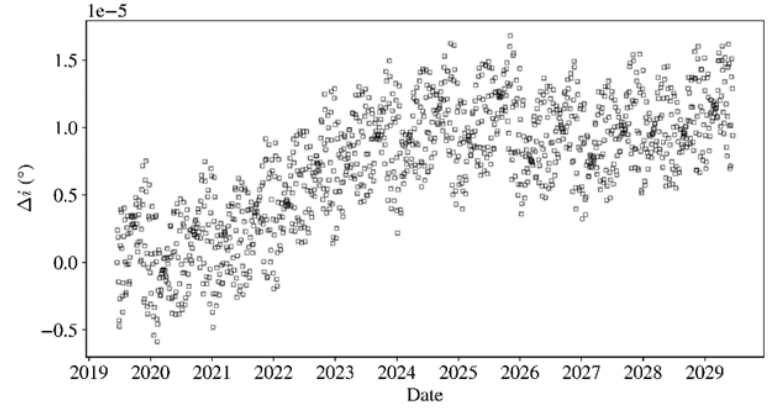

Figure 10. Difference Δi between the inclinations of the spherical and flat models.

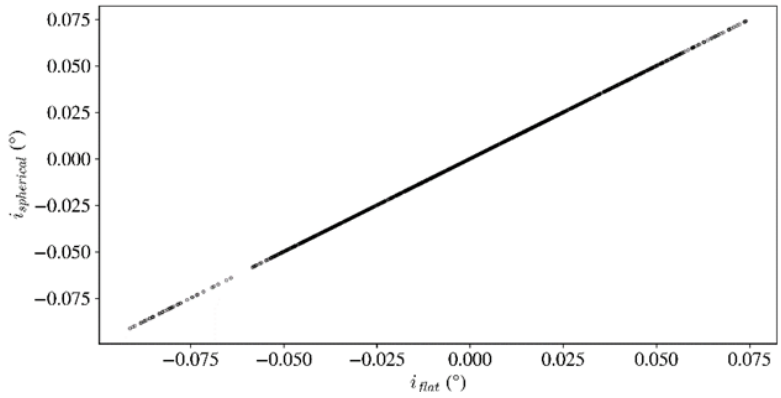

Figure 11. The relation between the inclinations of the spherical and flat models.

(penumbra). This coefficient modulates the SRP contribution of each plate according to its exposure to sunlight at a given time. The inputs necessary to generate orbital parameters using FreeFlyer are listed in Table 1. The input includes the average values of the orbital parameters from June 2019 to January 2023, the mass and dimensions of the geostationary satellite, the reflectivity coefficients and the moments of inertia based on the satellite's shape and an analytic atmospheric density model based on a constant-temperature hydrostatic model.

The spherical model estimates changes in the basic orbital parameters due to SRP, including variations in the satellite's semi-major axis, eccentricity, inclination, argument of perigee, right ascension of the ascending node, and mean anomaly. Although it does not capture all the intricacies of the behavior of a real geostationary (GEO) satellite, it nevertheless provides a foundational understanding of the way solar radiation affects these parameters. During the initial stages of mission planning, engineers often use the spherical model to estimate the perturbations caused by SRP. This knowledge facilitates the development of proactive collision-avoidance strategies, ensuring that GEO satellites maintain their precise positions and avoid space debris. However, real-world GEO satellites require more detailed simulations that consider factors such as the satellite shape, material properties, and orientation to create more accurate simulations. Such simulations enable engineers to make accurate adjustments to satellite trajectories, compensating for SRP-induced changes and ensuring that GEO satellites remain within their designated orbital parameters [21][22]. Equation (1) shows that the spherical model depends on the satellite mass, cross -sectional area, reflectivity coefficient, distance, and eclipse factor. The specific values for these parameters are listed in Table 1.

In contrast to the spherical model, the flat model considers differences in reflectivity and absorptivity across the various plates that make up the satellite's geometry. This results in variations in the acceleration caused by SRP that depend upon the satellite's orientation and geometry, and it allows for a more accurate representation of the effects of SRP on the satellite's motion and orbit [17][18][19]. Equation (2) shows that the flat model depends on the plate area, reflectivity coefficient, distance, and shadow coefficient, the detailed values for which are provided in Table 1.

Figure 1 illustrates the flat and spherical model configurations we assumed for the satellite in the present work. The flat model includes a central box (depicted in yellow in Figure 1a) and two solar panels (represented by blue "wings"). Figure 1b shows the spherical model, which represents the satellite as a uniform sphere. Further details regarding the model's dimensions are provided in Table 2. We also made the following assumptions about the satellite and its geometry. The "wings" are constructed of polished aluminum. The "wings" are consistently oriented to face the Sun (aligned with the Sun vector). The central box is always positioned to face the Earth. While these assumptions simplify the modeling process, it is important to note that the consistent Sun-pointing orientation of the solar panels is an idealization. In real-world operations, such alignment may be affected by various constraints, including periods of eclipse when the satellite is in Earth's shadow, as well as limitations in attitude control or onboard power availability. These factors can introduce deviations from the ideal orientation, which are not accounted for in the current model.

In satellite modeling, "articulation" refers to a satellite's ability to move or adjust its components relative to its main body. Articulation involves the movement of various components of the satellite, such as solar panels, antennas, instruments, or other deployable structures. These components may be capable of rotating or repositioning themselves relative to the satellite's main body. Articulation is important for modeling the satellite's attitude and orientation accurately, as this can affect its performance and behavior in its operational environment. The different types of articulation we consider here are as follows, Articulation model 0 assumes that the solar panels are fixed. Articulation model 1 assumes that the solar panels can rotate about a single axis to track the Sun. Articulation model 2 assumes that the solar panels can rotate about two axes for perfect sun tracking.

The SRP area "A" is the cross-sectional area of the satellite relative to the Sun–Earth line; it is necessary for calculating the force exerted on the satellite due to SRP. Because it determines the

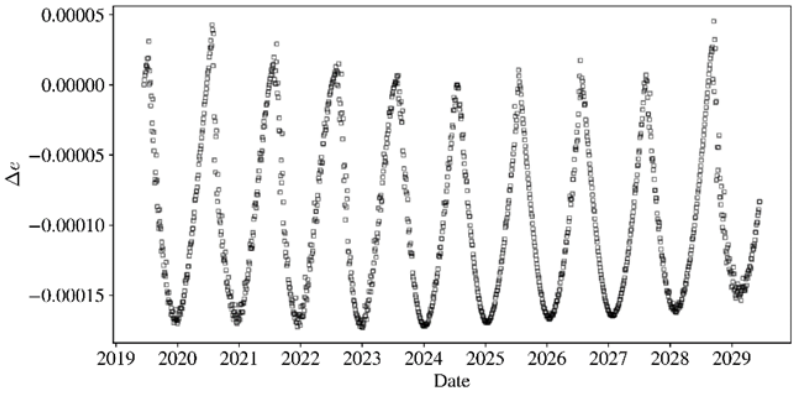

Figure 12. Difference Δ*e* between the eccentricities of the spherical and flat models.

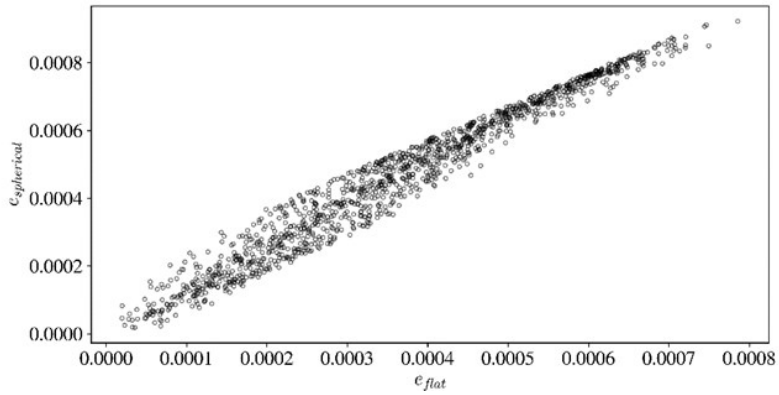

Figure 13. The relation between the eccentricities of the spherical and flat models.

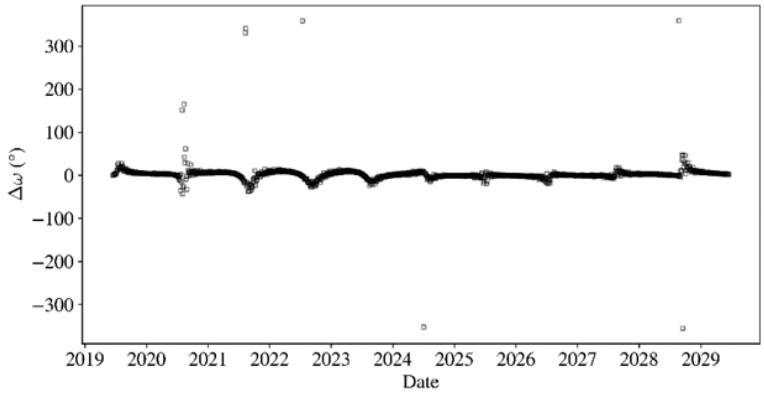

Figure 14. Difference Δω between the argument of perigee of the spherical and flat models.

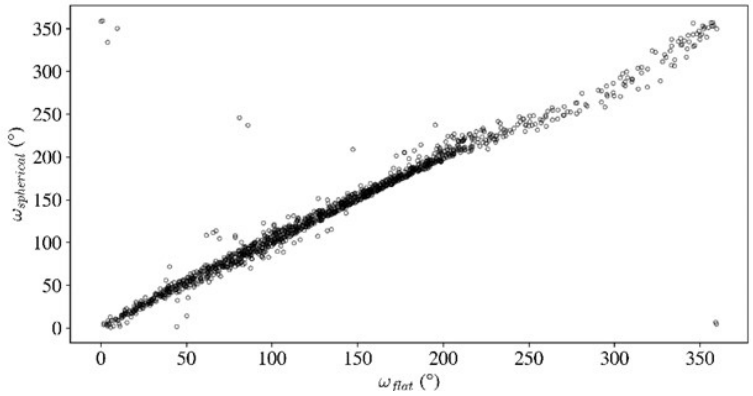

Figure15. The relation between the argument of perigee of the spherical and flat models.

magnitude of the force exerted by SRP on the satellite, it is thus a significant parameter for the design and analysis of satellite missions. The value of the SRP area depends upon the satellite's shape and orientation. Figures 2 (a), (b), and (c) compare the SRP area of the spherical model with those of the flat model using different articulation models (0, 1, and 2). In these figures, the spherical model of the satellite's shape exhibits a constant value of the SRP area because the cross-sectional area exposed to solar radiation does not vary. Notably, only for articulation model 2 does the flat model exceed the spherical model, while in the other articulation models, the values remain below those of the spherical model. The variations of SRP area in the flat model over a period of 10 years are 14.53% for articulation model 0, 3.66% for articulation model 1, and 3.56% for articulation model 2. This demonstrates that single-axis and dual-axis tracking improve SRP stability by minimizing the variation in exposed area.

The force "*F*" is due to SRP on a satellite's surface, which results from the momentum transferred from the photons in sunlight to the satellite's surface. As shown in Equation (1), it depends upon the satellite's cross-sectional area, reflectivity coefficient, distance from the Sun, and eclipse factor. These forces are shown in Figures 3 (a), (b), and (c), respectively, for the three different articulation models (0, 1, and 2). Notably, Figure 3 (c) (articulation model 2) exhibits a sharp pattern at the bottom of the figure. The variations in force over 10 years are 9.69% for articulation model 0, 6.75% for articulation model 1, and 6.44% for articulation model 2. These results confirm that solar tracking reduces SRP induced force variation, improving the satellite's stability.

In FreeFlyer, "energy" refers specifically to the instantaneous specific energy (energy per unit mass) of the satellite orbit. Based on the Keplerian gravitational potential, the specific energy is given by Equation (3);

$$E = \frac{-\mu}{2a} \quad (3)$$

Where μ is the gravitational parameter of the central body, and a is the semi-major axis of the satellite's orbit. The energy of a satellite is determined by its orbital characteristics, including the apogee, perigee, and eccentricity. Analyzing the evolution of a satellite's energy enables one to determine whether the satellite will maintain its intended orbit or whether propulsive maneuvers remain on course. Figures 4(a), (b), and (c) illustrate the energy obtained using different articulation models (0, 1, and 2). When the solar panels are fixed, the energy decreases gradually, with a minor periodic pattern superimposed (see Figure 4(a)). However, when the solar panels can rotate either about a single axis or about two axes, the energy exhibits only periodic changes, with no long-term secular variations (see Figures 4(b) and (c)). Over a 10-year period, the secular energy variations are 0.0029% for articulation model 0, while both articulation models 1 and 2 exhibit similar periodic variations with amplitudes of 0.0031%.

Torque refers to the rotational force acting on a satellite. It can be produced by various factors, including gravitational forces from celestial bodies, magnetic fields, and SRP. The force also can exert a torque on the satellite, which can be computed in the body-fixed frame of the satellite. The torque calculation takes into the satellite's geometry and reflectivity properties and the incident solar radiation. The torque plays a key role in determining the satellite's attitude and orientation, which are vital for satellite mission analysis and design. Additionally, the torque information can be utilized to optimize the output of a satellite's attitude-control system. Figures 5(a), (b), and (c), show the torque "τ" obtained for the three different articulation models (0, 1, and 2). Articulation model 2 exhibits much more pronounced periodic torque variations than the other articulation models (see Figure 5(c)). Over a 10-year period, the torque due to SRP varies by 55.35% for articulation model 0, 56.87% for articulation model 1, and 16.15% for articulation model 2. Although model 2—featuring dual-axis solar panel articulation—demonstrates a substantial reduction in torque variation compared to the other models, the remaining 16.15% variation is not negligible. In the context of geostationary satellites, such a level of torque fluctuation is generally considered manageable, particularly when supported by onboard attitude control systems such as reaction wheels or control moment gyroscopes. However, depending on the satellite's mission

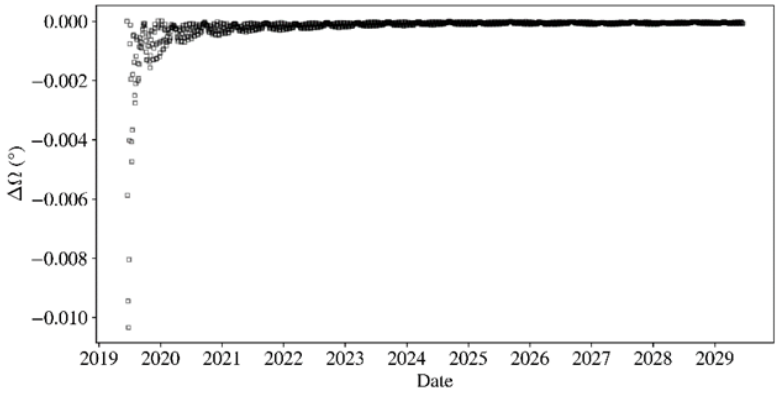

Figure 16. Difference ΔΩ between the right ascension of the ascending node of the spherical and flat models.

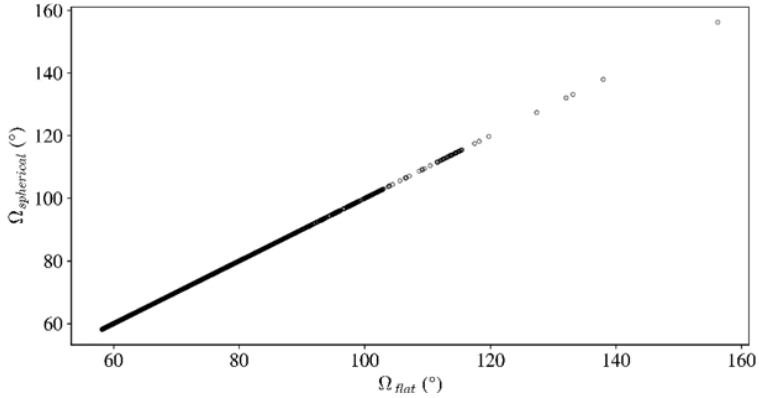

Figure 17. The relation between the right ascension of the ascending node of the spherical and flat models.

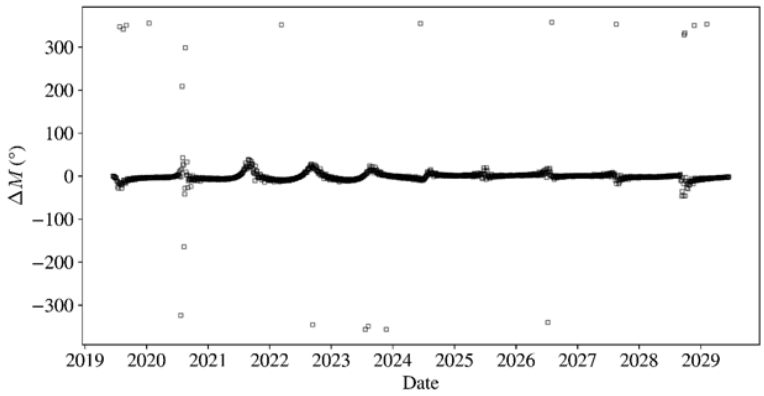

Figure 18. Difference Δ*M* between the mean anomalies of the spherical and flat models.

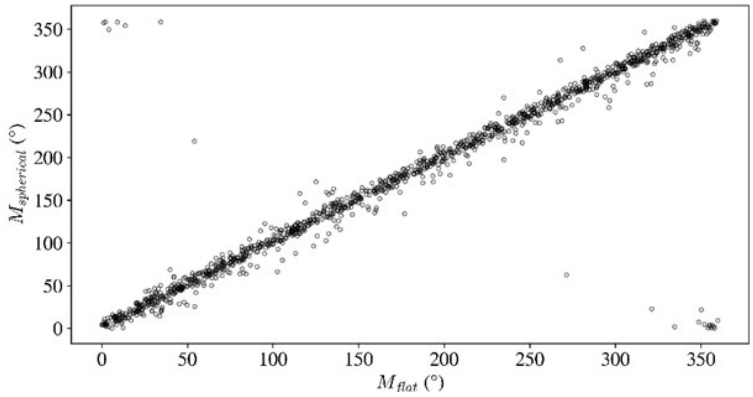

Figure 19. The relation between the mean anomalies of the spherical and flat models.

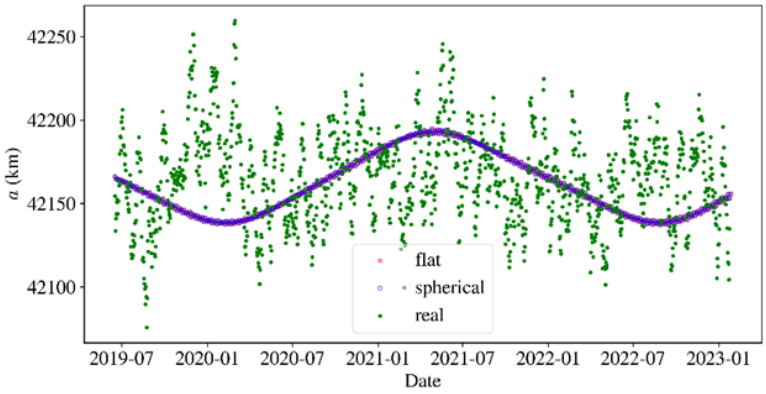

Figure 20. Comparison of the semi-major axes "*a*" for the flat (red) and spherical (blue) models with the data (green).

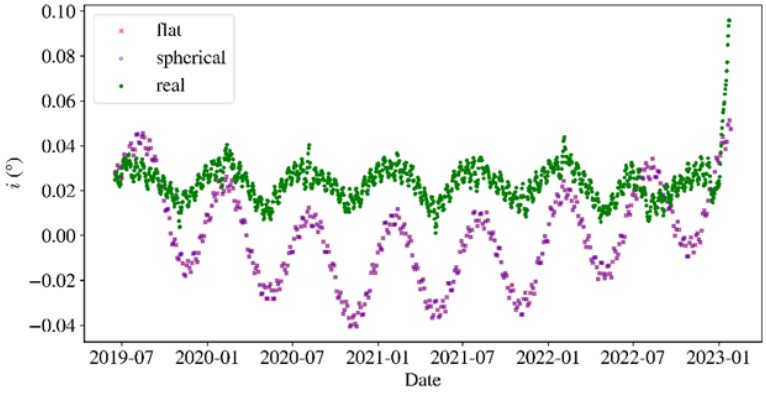

Figure 21. Comparison of the inclinations "*i*" for the flat (red) and spherical (blue) models with the data (green).

requirements, structural configuration, and available control authority, this residual torque may still require mitigation strategies. These could include periodic attitude corrections, incorporation of SRP-torque compensation algorithms in the attitude control system, or structural damping mechanisms. Therefore, while model 2 significantly improves SRP torque stability, operational planning should still consider this variation to ensure long-term pointing accuracy and momentum management in geostationary orbit.

In contrast, model 1, which uses single-axis articulation (e.g., pitch-only rotation), exhibits the highest torque variation at 56.87%, even exceeding the variation in the non-articulated model 0. This counterintuitive result occurs because the partial alignment of the panels with the Sun introduces dynamic asymmetries in SRP exposure, leading to unstable and unbalanced torque profiles over time. From an operational standpoint, such high torque variability can significantly increase the burden on attitude control systems, potentially accelerating the depletion of fuel for thruster-based momentum dumping or reducing the lifespan of reaction wheels due to frequent corrections. Moreover, sustained torque oscillations may impact satellite pointing stability, particularly for payloads requiring precise geolocation or antenna alignment. Therefore, while model 1 offers some energy capture benefits, it poses long-term viability challenges without additional design considerations or control strategies to manage the elevated torque dynamics.

Orbital velocity is a fundamental parameter in satellite dynamics, directly reflecting the balance between gravitational and perturbative forces acting on the spacecraft. Its evolution is governed by the underlying force models used in orbit propagation, including gravitational harmonics, SRP, and atmospheric drag. Monitoring changes in velocity over time is essential for assessing orbital stability and detecting deviations that may necessitate corrective maneuvers, such as station-keeping or attitude adjustments. Figures 6(a), (b), and (c), display the velocity "*v*" obtained using the three

articulation models (0, 1, and 2). When the solar panels are fixed, the velocity increases gradually, with a minor periodic pattern superimposed. However, when the solar panels can rotate either about a single axis or about two axes, the velocity exhibits only similar periodic changes. Over 10 years, the variations in the velocity are 0.02% for all articulation models (a secular change for model 0, and the amplitude of the periodic variations for models 1 and 2).

The acceleration experienced by a satellite depends upon the forces acting on it, including gravitational attraction, SRP, and aerodynamic drag. Figures 7(a), (b), and (c) display the acceleration "*acc*" obtained using the three articulation models (0, 1, and 2). The patterns in these figures are similar to those of the velocities (shown in Figures 6(a), (b), and (c) but with a narrower range of values. Over 10 years, the secular variations in acceleration are 0.02% for articulation model 0, while both articulation models 1 and 2 exhibit periodic variations with similar amplitudes of 0.04%. These results suggest that single-axis and dual-axis tracking introduce periodic perturbations but reduce long-term secular drift.

3. COMPARISON OF THE ORBITAL PARAMETERS OBTAINED USING THE SPHERICAL AND FLAT MODELS IN FREEFLYER

In this section, we compare the orbital parameters obtained from the spherical model with those obtained from a flat model using articulation model 2 for precise sun tracking. The semi-major axis "*a*" determines an orbit's size; it is approximately the average distance between the satellite and Earth. Typically, this parameter remains very stable and exhibits low sensitivity to perturbations. Figure 8 illustrates the differences Δa between spherical and flat models. The maximum difference between the spherical and flat models amounts to roughly 0.022 km, with a standard deviation of about 0.01. Not surprisingly, both

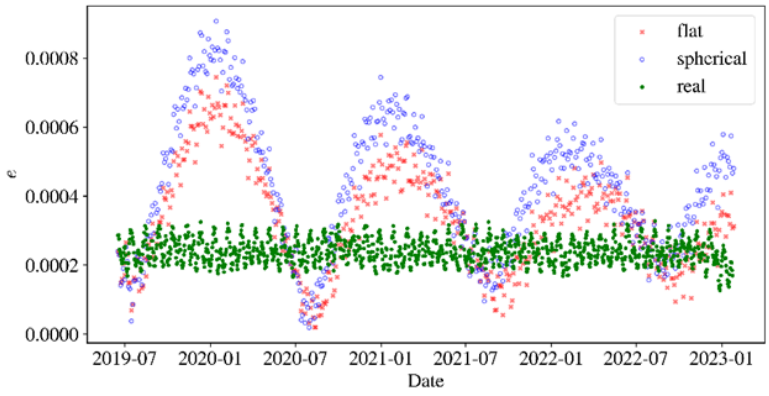

Figure 22. Comparison between the eccentricities "*e*" of the flat (red) and spherical (blue) models with those obtained from the real data (green).

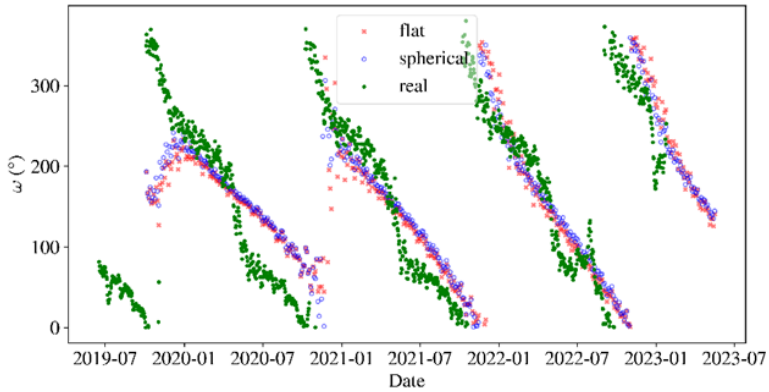

Figure 23. Comparison of the argument of perigee "ω" for the flat (red) and spherical (blue) models with that for the real data (green).

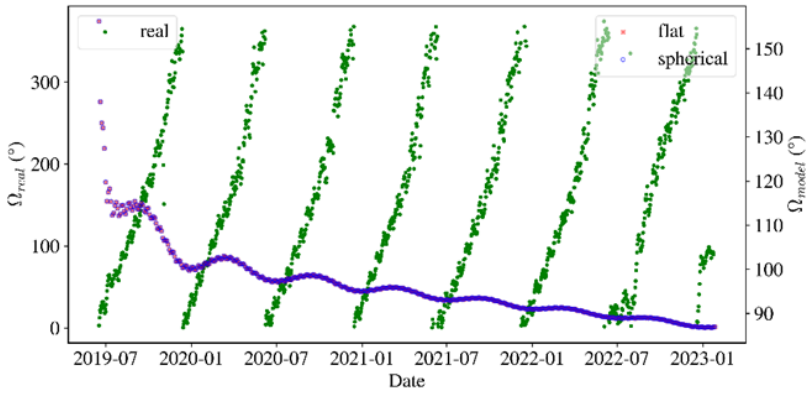

Figure 24. Comparison of the right ascension of the ascending node "Ω" for the flat (red) and spherical (blue) models with the data (green).

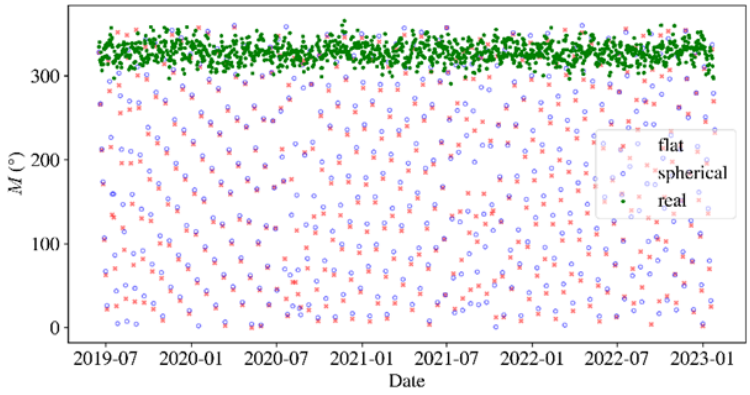

Figure 25. Comparison of the mean anomalies "*M*" of the flat (red) and spherical (blue) models with those obtained from the data (green).

models exhibit strikingly similar variations, as evidenced by the high Pearson correlation coefficient of approximately 0.99, as shown in Figure 9. This high correlation coefficient indicates a strong linear relationship between the variations of the spherical and flat models.

The inclination "*i*" of the satellite orbit is the angle at which the orbital plane is tilted relative to the equatorial plane. While it is generally stable, external perturbations can induce a gradual precession of the orbital plane over time. The magnitude of the precession depends upon the system's mass distribution. Figure 10 shows the difference Δi between the spherical and flat models, with the maximum observed difference amounting to approximately 0.000017°. The difference between the two models has a standard deviation of about 0.000005°. Here also the Pearson correlation coefficient is 0.99, denoting a perfect correlation between these models, as shown in Figure 11.

The eccentricity "*e*" defines an orbit's shape, ranging from a circular orbit with $e = 0$ to an elongated elliptical form. This parameter is highly sensitive to minute perturbations, with even slight alterations in eccentricity resulting in significant changes in the shape, orientation, and size of an orbit. Discernible differences are apparent between them in Figure 12, with the maximum difference reaching $\Delta e \approx 0.000045$. The difference between the two models has a standard deviation of about 0.000058. Both models exhibit similar patterns in their variations, with a Pearson correlation coefficient of approximately 0.98, as shown in Figure 13.

The argument of perigee "ω" defines the orientation of an orbit within its orbital plane, and it is also sensitive to perturbations. Discernible differences between the two models are shown in Figure 14, with the maximum observed difference reaching approximately 358.34°. The difference $\Delta\omega$ between the two models has a standard deviation of about 25.99°. Their variations exhibit similar patterns, with a Pearson correlation coefficient of 0.94, as shown in Figure 15.

The right ascension of the ascending node "Ω" marks the point where an orbit intersects the ecliptic plane, as measured from a reference direction. Its susceptibility to perturbations depends upon the mass distribution and gravitational interactions within the system. Discernible differences between the spherical and flat models are shown in Figure 16, with the maximum observed difference reaching $\Delta\Omega \approx 0.000018°$. The difference between the two models has a standard deviation of about 0.000574°. Again, these variations are very similar, with a high Pearson correlation coefficient of about 0.99, as shown in Figure 17.

The mean anomaly "*M*" denotes the angular position of an orbiting body along its elliptical path at a specific moment in time. Its linear progression over time remains consistent regardless of the shape of the orbit. While the mean anomaly itself is not especially susceptible to perturbations, it significantly influences the true anomaly, which characterizes the actual angular position of the body at any given time. The differences between these models are apparent in Figure 18, with the maximum observed disparity reaching approximately 357.66°. The difference between the two models has a standard deviation of about 43.37. Again, these variations exhibit similar patterns, with a Pearson correlation coefficient of around 0.91, as shown in Figure 19.

4. COMPARISON OF THE ORBITAL PARAMETERS FROM THE SPHERICAL AND FLAT MODELS WITH THE DATA

After comparing the spherical and flat models generated using FreeFlyer, we next compare these simulations with actual empirical data to evaluate and validate their accuracy and reliability in replicating real-world orbital parameters. The real data used in this study were obtained from publicly available two-line element (TLE) sets provided by Celestrak, which are updated regularly—typically every few days—to reflect the latest tracking information. These TLEs offer a practical representation of satellite orbits and are widely used for operational and analytical purposes, although they are subject to observational limitations and modeling approximations. Comparing the simulation results with TLE-derived data allows us to assess how well each model captures the dynamics observed in the satellite's actual trajectory.

Figure 20 illustrates the evolution of the semi-major axis over time, comparing simulated results using flat and spherical Earth models with real data from TLE. While the models closely track the general periodic trend, the real data exhibit significantly more scatter. This scatter arises from both physical and observational factors. Physically, real satellite orbits are influenced by complex perturbations such as third-body effects (e.g., lunar and solar gravity), SRP, Earth's non-uniform gravity field, and occasional station-keeping maneuvers. Observationally, the use of TLEs contributes additional variability: TLEs provide mean orbital elements rather than instantaneous osculating ones, and their limited precision, infrequent updates, and reliance on the simplified SGP4 propagator introduce modeling artifacts.

Figure 21 compares the inclinations "*i*" obtained from the flat and spherical models with those obtained from the real data. Both the models and the real data exhibit similar periodic patterns, with almost all maxima occurring on the same dates. The real data indicate relatively stable and minor oscillations in inclination with a notable increase towards the end of the observed period, suggesting a potential maneuver or perturbative event. The flat and spherical models exhibit more pronounced cyclic variations, reflecting perturbative effects. The discrepancy between the model predictions and the real data, may be attributed to routine inclination correction maneuvers performed on the satellite to maintain it within a specified operational range.

Figure 22 compares the eccentricities "*e*" obtained from the spherical model, the flat model, and the real data. The real data exhibit a stable and low eccentricity, while the flat and spherical models display significant cyclical variations. The comparison indicates that while the models successfully capture periodic perturbative effects on eccentricity, they do not account for certain stabilizing influences—such as station-keeping maneuvers or operational constraints—that are present in the real-world data. Figure 23 compares the argument of perigee "*ω*" of the spherical and flat models with that from the real data. The real

data show a clear cyclic pattern of linear decreases and resets, indicative of orbital perturbations and periodic adjustments. The flat and spherical models closely mimic this trend, showing their effectiveness in capturing the key dynamics of the satellite's orbit.

Figure 24 compares the right ascension of the ascending node "Ω" as derived from the spherical and the flat models with that obtained from the real data. The real data show periodic variations, likely due to gravitational perturbations, while the models show a smooth, gradual decrease, capturing the general trend. Figure 25 compares the mean anomalies "*M*" derived from the spherical model and the flat model with those obtained from the real data. The real data show a narrow range of mean anomaly values, suggesting stable orbital characteristics, while the flat and spherical models predict a wider range of values, indicating more variability.

5. CONCLUSIONS

This study demonstrates that SRP significantly influences the long-term orbital evolution of geostationary satellites and that the choice of articulation model plays a crucial role in mitigating its effects. Among the three models evaluated, the flat model with dual-axis tracking (model 2) provides the most stable and consistent orbital behavior, particularly in reducing SRP-induced perturbations such as torque and force variations. Furthermore, the comparison between the spherical and flat models shows strong agreement, with high correlations across all orbital parameters and close alignment with real observational data, despite minor discrepancies. These findings highlight the effectiveness of model 2 in enhancing orbital stability, offering valuable guidance for the design and operation of future geostationary satellites, especially in optimizing solar panel articulation strategies and refining station-keeping maneuvers.

AUTHOR INFORMATION

Corresponding Author

Nindhita Pratiwi — Atmospheric and Planetary Science Department, Institut Teknologi Sumatera, Lampung Selatan-35365 (Indonesia); Astronomy Department, Institut Teknologi Bandung, Bandung-40132 (Indonesia);
orcid.org/0009-0008-9631-216X
Email: nindhita.pratiwi@sap.itera.ac.id

Authors

Dhani Herdiwijaya — Astronomy Department, Institut Teknologi Bandung, Bandung-40132 (Indonesia);
orcid.org/0000-0001-6630-8735

Nizam Ahmad — Research Center for Smart Mechatronics, The National Research and Innovation Agency (BRIN), Bandung-40135 (Indonesia);
orcid.org/0000-0001-7842-1946

Taufiq Hidayat — Astronomy Department, Institut Teknologi Bandung, Bandung-40132 (Indonesia);
orcid.org/0009-0008-8045-6054

Muhammad Isnaenda Ikhsan — Atmospheric and Planetary Science Department, Institut Teknologi Sumatera, Lampung Selatan-35365 (Indonesia); Astronomy Department, Institut Teknologi Bandung, Bandung-40132 (Indonesia);
orcid.org/0009-0004-1346-3503

Author Contributions

Conceptualization, N. P. and D. H.; Methodology, Formal Analysis, Investigation, Data Curation, Project Administration, Funding Acquisition, Writing – Original Draft Preparation, Writing – Review & Editing, N. P.; Software, and Visualization, M. I. I.; Validation, D. H., N. A. and T. H.; Resources, D. H.; Supervision, D. H. and N. A.

Conflicts of Interest

The authors declare no conflict of interest.

ACKNOWLEDGEMENT

This research supported by Institut Teknologi Sumatera (ITERA), Institut Teknologi Bandung (ITB), and National Research and Innovation Agency (BRIN). We extend our gratitude to Dr. T.S. Kelso (CelesTrak-NORAD) and WDC for Geomagnetism Kyoto (Japan), for providing open access to the data for scientific research.

REFERENCES

[1] B. Duan, and U. Hugentobler. (2021). "Enhanced solar radiation pressure model for GPS satellites considering various physical effects". *GPS Solutions*. 25. 10.1007/s10291-020-01073-z

[2] A. Mostafa, M. I. El-Saftawy, E. I. Abouelmagd, and M. A. Lopez. (2020). "Controlling the perturbations of solar radiation pressure on the Lorentz spacecraft". *Symmetry*. **12** (9): 1423. 10.3390/sym12091423

[3] S. Lupu, and E. Zaharescu. (2014). "Effects of direct and indirect solar radiation pressure in orbital parameters of GPS satelittes". *Analele Stiintifice ale Universitatii Ovidius Constanta, Seria Matematica*. **22** (2): 141-150. 10.2478/auom-2014-0039

[4] Z. Li, and M. Ziebart. (2020). "Uncertainty analysis on direct solar radiation pressure modeling for GPS IIR and Galileo FOC satellites". *Advances in Space Research*. **66** (4). 10.1016/j.asr.2020.04.050

[5] E. R. Burnett, and H. Schaub. (2021). "Spacecraft formation and orbit control using differential attitude-dependent solar radiation pressure". *Advances in Space Research*. **67** (11). 10.1016/j.asr.2020.03.047

[6] D. Henry. (2006). "Robust fault diagnosis of the Microscope satellite micro-thrusters". *IFAC Proceedings Volumes*. **6** : 342-347. 10.3182/20060829-4-CN-2909.00056

[7] I. Jean, A. Ng, and A. K. Misra. (2019). "Impact of solar radiation pressure modeling on orbital dynamics in the vicinity of binary asteroids". *Acta Astronautica*. 165. 10.1016/j.actaastro.2019.09.003

[8] J. A. Paris. (2006). "The effects of using solar radiation pressure to alleviate fuel requirements for orbit changing and maintenance of the DSCS II F-13 satellite". *Master's thesis Air Force Institute of Technology, Wright-Patterson Air Force Base, Ohio: Department of the Air Force, Air University*. 155.

[9] D. G. Cook. (2001). "Solar radiation pressure modeling issues for high altitude satellites". *Master's thesis. Air Force Institute of Technology, Wright-Patterson Air Force Base, Ohio: Department of the Air Force, Air University*. 148.

[10] X. Chang, B. Mannel, and H. Schuh. (2021). "An analysis of a priori and empirical solar radiation pressure models for GPS satellites". *Advances in Geosciences*. **55** : 33-45. 10.5194/adgeo-55-33-2021

[11] L. Tang, J. Wang, H. Zhu, M. Ge, A. Xu, and H. Schuh. (2021). "A comparative study on the solar radiation pressure modeling in GPS precise orbit determination". *Remote Sensing*. **13** (17): 3388. 10.3390/rs13173388

[12] N. Pratiwi, and D. Herdiwijaya. (2022). "Solar radiation pressure on LAPAN A1 satellite due to extreme geomagnetic storm". *Journal of Physics: Conference Series*. **2243** (1): 012013. 10.1088/1742-6596/2243/1/012013

[13] A. R. Fogg, C. M. Jackman, I. Coco, L. D. Rooney, D. M. Weigt, and M. Lester. (2023). "Why are some solar wind pressure pulses followed by geomagnetic storms?" *Journal of Geophysical Research: Space Physics*. **128** (8). 10.1029/2022JA031259

[14] M. A. Yousef, M. I. El-Saftawy, and A. Mostafa. (2022). "Balancing the effects of solar radiation pressure on the orbital elements of a spacecraft using Lorentz force". *Scientific Reports*. **12** (1). 10.1038/s41598-022-20166-y

[15] D. Mishne, and E. Edlerman. (2017). "Collision-avoidance maneuver of satellites using drag and solar radiation pressure". *Journal of Guidance, Control, and Dynamics*. **40** (5). 10.2514/1.G002376

[16] M. I. Rashed, and H. Bang. (2022). "A study of autonomous small satellite constellations for disaster management and deep space strategy". *Remote Sensing*. **14** (23): 6148. 10.3390/rs14236148

[17] K. Vielberg, and J. Kusche. (2020). "Extended forward and inverse modeling of radiation pressure accelerations for LEO satellites". *Journal of Geodesy*. **94** (4). 10.1007/s00190-020-01368-6

[18] A. Farres, C. Webster, and D. Folta. (2018).

"High fidelity modeling of SRP and its effect on the relative motion of Starshade and WFIRST". *Proceedings of the Space Flight Mechanics Meeting*. 2227. 10.2514/6.2018-2227

[19] C. P. Newman, J. R. Hollister, D. C. Davis, and E. M. Zimovan-Spreen. (2022). "Investigating Solar Radiation Pressure Modeling for Operations in Near Rectilinear Halo Orbit". *Proceedings of the Astrodynamics Specialists Conference*. 10382.

[20] D. A. Vallado. (2007). "Fundamentals of Astrodynamics and Applications, 3rd ed". Springer, Berlin.

[21] M. Lachut, and J. Bennett. (2016). "Towards Relaxing the Spherical Solar Radiation Pressure Model for Accurate Orbit Predictions". *Advanced Maui Optical and Space Surveillance Technologies Conference*. 49.

[22] P. Kelly, R. S. Erwin, R. Bevilacqua, and L. Mazal. (2016). "Solar Radiation Pressure Applications on Geostationary Satellites". *GNC AAS Conference*. **16** (012).